DC Josephson effect between two Yu-Shiba-Rusinov bound states

Subrata Chakraborty [1,*] Danilo Nikolić [1,2,†] Rubén Seoane Souto [3,4] Wolfgang Belzig [1] and Juan Carlos Cuevas [3]

[1]*Fachbereich Physik, Universität Konstanz, D-78457 Konstanz, Germany*
[2]*Institut für Physik, Universität Greifswald, Felix-Hausdorff-Strasse 6, 17489 Greifswald, Germany*
[3]*Departamento de Física Teórica de la Materia Condensada and Condensed Matter Physics Center (IFIMAC),
Universidad Autónoma de Madrid, E-28049 Madrid, Spain*
[4]*Instituto de Ciencia de Materiales de Madrid (ICMM), Consejo Superior de Investigaciones Científicas (CSIC),
Sor Juana Inés de la Cruz 3, 28049 Madrid, Spain*

Motivated by recent experiments [Nat. Phys. **16**, 1227 (2020)], we present here a theoretical study of the DC Josephson effect in a system comprising two magnetic impurities coupled to their respective superconducting electrodes and which exhibit Yu-Shiba-Rusinov (YSR) states. We make use of a mean-field Anderson model with broken spin symmetry to compute the supercurrent in this system for an arbitrary range of parameters (coupling between the impurities, orientation of the impurity spins, etc.). We predict a variety of physical phenomena such as (i) the occurrence of multiple 0-π transitions in the regime of weak coupling that can be induced by changing the energy of the YSR states or the temperature; (ii) the critical current strongly depends on the relative orientation of the impurity spins and it is maximized when the spins are either parallel or antiparallel, depending on the ground state of the impurities; and (iii) upon increasing the coupling between impurities, triplet superconductivity is generated in the system and it is manifested in a highly nonsinusoidal current-phase relation. In principle, these predictions can be tested experimentally with the existing realization of this system and the main lessons of this work are of great relevance for the field of superconducting spintronics.

I. INTRODUCTION

The advent of scanning tunneling microscopy (STM) has enabled the investigation of the interplay between magnetism and superconductivity at the atomic scale in the context of single magnetic impurities on superconducting surfaces [1,2]. One of the most emblematic manifestations of this interplay is the appearance of in-gap superconducting bound states, known as Yu-Shiba-Rusinov (YSR) states [3–5]. These bound states can induce a quantum phase transition in which the ground state of the impurity system may change between a singlet state (spin 0) and a double state (spin 1/2) [6–10]. The change in fermion parity in this transition is accompanied by a supercurrent reversal in Josephson junctions, often referred to as 0-π transition. This kind of transition has been reported in different mesoscopic systems ranging from superconductor-ferromagnet hybrid junctions [11–16] to single [17–22] and double [23–32] quantum dots coupled to superconducting leads. However, in the context of STM-based experiments with magnetic impurities on superconductor substrates, it has been very elusive to observe a 0-π transition due to the lack of phase sensitivity in this type of setup. This was recently circumvented with the help of the presence of a second channel in an experiment featuring a single YSR pair of states in a vanadium-based system [33].

In this work we focus on a system in which two magnetic impurities are coupled to their respective superconducting electrodes such that one can have quantum tunneling between two individual YSR states, see Fig. 1(a). This system has been recently realized experimentally in the context of STM and it constitutes the ultimate limit of quantum tunneling [34]. In those experiments the authors focused on the current-voltage characteristics and the results have been understood with the help of mean-field models that account for the relative orientation between the impurity spins [35–37]. Here, we shall focus on the DC Josephson effect and employ the mean-field model to make concrete predictions for the current-phase relation and the critical current in this two-impurity system. Our study is motivated by the fact that this system is an ideal playground to investigate fundamental questions in the field of superconducting spintronics [38,39]. In particular, we predict that the supercurrent in this hybrid atomic-scale system exhibits a number of spin-related phenomena among which we can highlight (i) the occurrence of multiple 0-π transitions in the tunneling regime (weak coupling between the impurities) that can be induced by changing the position of the YSR states or by modifying the temperature; (ii) the critical current depends drastically on the relative orientation of the impurity spins and it is maximized either when the impurity spins are parallel or antiparallel, depending on the ground state of the impurities; (iii) upon increasing the coupling between the impurities, triplet superconductivity is generated and is revealed in a highly nonsinusoidal current-phase relation. These predictions could be tested experimentally using the exact system

*Corresponding author: subrata.chakraborty@uni-konstanz.de
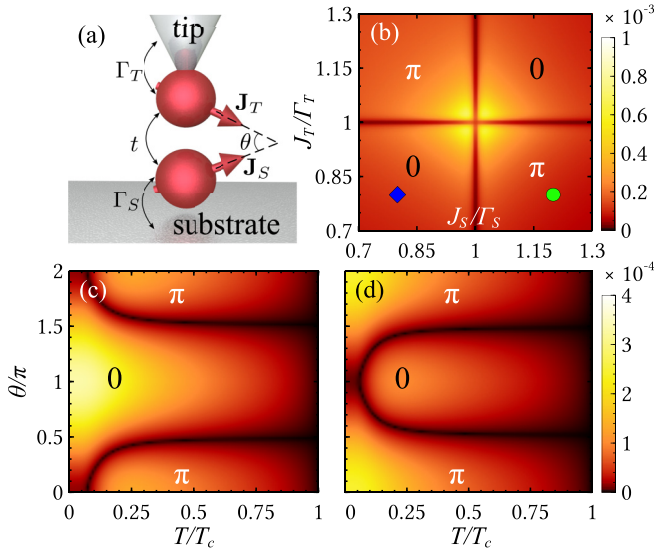†danilo.nikolic@uni-konstanz.de

094518-1

FIG. 1. (a) Schematic representation of the system under study. Two magnetic impurities with exchange fields J_S and J_T forming an angle θ are respectively coupled to a superconducting substrate and to a superconducting STM tip. The tunneling rates Γ_T and Γ_S measure the strength of the coupling of the impurities to the tip and substrate, respectively, and t is the hopping matrix element describing the tunnel coupling between the impurities. (b) The zero-temperature critical current as a function of the ratios J_S/Γ_S and J_T/Γ_T for $\theta = \pi/2$. In panel (b), we mark ($J_S/\Gamma_S = 0.8, J_T/\Gamma_T = 0.8$) (blue colored diamond shaped) and ($J_S/\Gamma_S = 1.2, J_T/\Gamma_T = 0.8$) (green colored circular shaped) points. (c) The critical current as a function of the temperature and the angle θ for $J_S/\Gamma_S = J_T/\Gamma_T = 0.8$. (d) The same quantity as in panel (c), but for $J_S/\Gamma_S = 1.2$ and $J_T/\Gamma_T = 0.8$. For panels (b)–(d) $t = \Delta_0$, $\Gamma_{S/T} = 100\Delta_0$, $U_{S/T} = 0$, and $\gamma = 0.003\Delta_0$. The critical currents with color maps in panels (b)–(d) are expressed in the units of $e\Delta_0/\hbar$.

of Ref. [34] and our main conclusions have important implications for the whole field of superconducting spintronics.

The rest of the paper is organized as follows. First, in Sec. II we present our theoretical model to describe the coupling between two YSR states, and provide a prescription to compute the DC Josephson current between the two states. Then, in Sec. III we discuss our main results on the 0-π transitions in the supercurrent for low transmissions, the emergence of triplet superconductivity and how it is reflected in the supercurrent, and the appearance of higher order harmonics in the current-phase relation beyond the tunnel regime. We summarize the main conclusions of this work in Sec. IV. Some of the technical details related to the supercurrent in the tunneling regime are reported in Appendix A, while a discussion of the critical current in the case of nonorthogonal spin orientations is presented in Appendix B.

II. MODEL

A. System

To study the supercurrent between two YSR states, we consider the two-impurity system schematically represented in Fig. 1(a). Here, a magnetic impurity is attached to a superconducting substrate (S) and another impurity decorates

a superconducting STM tip (T). The system was already realized in Refs. [34,36]. Because of the strong coupling to their respective superconducting electrodes, both impurities exhibit a pair of YSR states. In turn, both impurities are tunnel coupled, which causes YSR hybridization and the corresponding supercurrent flow when a phase difference is established across the junction. To describe this system, we make use of the mean-field model used in Ref. [35], which is summarized by a Hamiltonian given by $\hat{\bar{H}} = \hat{\bar{H}}_S + \hat{\bar{H}}_T + \hat{\bar{V}}$. Here, $\hat{\bar{H}}_{S,T}$ describes the subsystem formed by an impurity attached to the superconductor $j = S, T$ and $\hat{\bar{V}}$ describes the coupling between the magnetic impurities. With respect to the global spin-quantization axis, defined as the middle angle between $\mathbf{J}_T$ and $\mathbf{J}_S$, we can choose the basis set for an impurity attached to the respective superconductor $j = S, T$ given by $\bar{d}_j^\dagger = (\bar{d}_{j\uparrow}^\dagger, \bar{d}_{j\downarrow}, \bar{d}_{j\downarrow}^\dagger, -\bar{d}_{j\uparrow})$. For the superconducting electrodes we choose a basis set with respect to the global spin-quantization frame as $\bar{c}_{\mathbf{k}j}^\dagger = (\bar{c}_{\mathbf{k}j\uparrow}^\dagger, \bar{c}_{\mathbf{k}j\downarrow}, \bar{c}_{\mathbf{k}j\downarrow}^\dagger, -\bar{c}_{\mathbf{k}j\uparrow})$. The Hamiltonian of a bare YSR system, i.e., a magnetic impurity plus the corresponding superconductor is expressed in the above basis as $\hat{\bar{H}}_j = \hat{\bar{H}}_{\text{elec},j} + \hat{\bar{H}}_{\text{imp},j} + \hat{\bar{H}}_{\text{int},j}$, where

$$\hat{\bar{H}}_{\text{imp},j} = \frac{1}{2}\bar{d}_j^\dagger \, \bar{H}_{\text{imp},j} \, \bar{d}_j, \tag{1}$$

$$\hat{\bar{H}}_{\text{elec},j} = \frac{1}{2}\sum_{\mathbf{k}} \bar{c}_{\mathbf{k}j}^\dagger \, \bar{H}_{\text{elec},\mathbf{k}j} \, \bar{c}_{\mathbf{k}j}, \tag{2}$$

$$\hat{\bar{H}}_{\text{int},j} = \frac{1}{2}\sum_{\mathbf{k}} \bar{c}_{\mathbf{k}j}^\dagger \, \bar{H}_{\text{int},j} \, \bar{d}_j + \text{H.c.} \tag{3}$$

In Eqs. (1)–(3) the Hamiltonian matrices are given by $\bar{H}_{\text{imp},j} = U_j(\sigma_0\tau_3) + \mathbf{J}_j \cdot (\boldsymbol{\sigma}\tau_0)$, $\bar{H}_{\text{elec},\mathbf{k}j} = \sigma_0(\xi_{\mathbf{k}j}\tau_3 + \Delta_j e^{i\phi_j\tau_3}\tau_1)$, and $\bar{H}_{\text{int},j} = v_j(\sigma_0\tau_3)$. They define the bare magnetic impurity attached to the respective superconductor j, the corresponding superconducting electrode j, and the interaction between them, respectively. These Hamiltonian matrices are expressed in spin $\otimes$ Nambu space $\sigma_i\tau_j$, where σ_i and τ_j denote the Pauli matrices in the respective space. The superconductors are described by electronic energy $\xi_{\mathbf{k}j}$, pairing potential Δ_j, and superconducting phase ϕ_j. The bare magnetic impurities are described by the single-particle energy U_j and the exchange field $\mathbf{J}_j$. An important parameter of this model is the angle θ describing the relative orientation between the two impurity spins, i.e., between $\mathbf{J}_S$ and $\mathbf{J}_T$. The strength of the coupling between an impurity and its corresponding superconductor is denoted by v_j. Due to the hybridization between the two YSR systems, the tunneling Hamiltonian in the above basis adopts the form

$$\hat{\bar{V}} = \tfrac{1}{2}\bar{d}_T^\dagger \bar{V}_{TS}\bar{d}_S + \tfrac{1}{2}\bar{d}_S^\dagger \bar{V}_{ST}\bar{d}_T, \tag{4}$$

where $\bar{V}_{TS} = t(\sigma_0\tau_3) = \bar{V}_{ST}$, and t is the hopping matrix element that describes the strength tunneling between the two YSR subsystems. The tunneling Hamiltonian $\hat{\bar{V}}$ accounts for the spin-independent tunneling processes. However, spin-flip process will effectively take place when the spins are misaligned, as we explain in what follows.

Instead of working with a global spin-quantization frame, for convenience, we use mixed quantization axes such that S and T subsystems are spin-quantized along the exchange fields $\mathbf{J}_S$ and $\mathbf{J}_T$, respectively. For this purpose we make

use of the rotation matrix for subsystem $j = S, T$ as $R_j = \exp(i\theta_j \sigma_2/2)\tau_0$, where $\theta_{T/S} = \pm\theta/2$ is the relative angle of the exchange fields $\mathbf{J}_{T/S}$ with respect to the global quantization axis. Upon rotation, we can define the basis along the respective exchange field directions as $d_j^\dagger = R_j \bar{d}_j^\dagger \equiv$

$(d_{j\uparrow}^\dagger, d_{j\downarrow}, d_{j\downarrow}^\dagger, -d_{j\uparrow})$. Due to the superconductor-impurity coupling, the dressed retarded/advanced (r/a) Green's function matrix of each impurity in the basis $d_j^\dagger$ becomes $g_{jj}^{r/a}(E) = g_{jj\uparrow\uparrow}^{r/a}(E) \oplus g_{jj\downarrow\downarrow}^{r/a}(E)$ with

$$g_{jj\sigma\sigma}^{r/a}(E) = \frac{1}{D_{j\sigma}(E)}\begin{pmatrix} E\Gamma_j + (E + U_j - J_{j\sigma})\sqrt{\Delta_j^2 - E^2} & \Gamma_j \Delta_j e^{i\phi_j} \\ \Gamma_j \Delta_j e^{-i\phi_j} & E\Gamma_j + (E - U_j - J_{j\sigma})\sqrt{\Delta_j^2 - E^2} \end{pmatrix}, \quad (5)$$

where $\Gamma_j = \pi N_{0,j} v_j^2$ ($N_{0,j}$ being the normal density of states of electrode j), $D_{j\sigma}(E) = 2\Gamma_j E(E - J_{j\sigma}) + [(E - J_{j\sigma})^2 - U_j^2 - \Gamma_j^2]\sqrt{\Delta_j^2 - E^2}$, and $E = E \pm i\gamma$ (with $\gamma \to 0^+$). Here, $J_{j\uparrow} = +J_j$ and $J_{j\downarrow} = -J_j$. The YSR bound states can be obtained by setting $D_{j\sigma}(E) = 0$ for $J_j, \Gamma_j \gg \Delta_j$, and they are expressed as $E_{\mathrm{YSR},j\uparrow} = -E_{\mathrm{YSR},j\downarrow}$ with

$$E_{\mathrm{YSR},j\uparrow} = \Delta_j \frac{J_j^2 - \Gamma_j^2 - U_j^2}{\sqrt{[\Gamma_j^2 + (J_j - U_j)^2][\Gamma_j^2 + (J_j + U_j)^2]}}. \quad (6)$$

For $U_j = 0$ it is easy to show that if $J_j/\Gamma_j \lessgtr 1$, then $E_{\mathrm{YSR},j\uparrow} = -E_{\mathrm{YSR},j\downarrow} \lessgtr 0$. Next, to study the supercurrent between the two impurities we need the tunneling matrices with respect to the mixed quantization frames. The tunneling matrices are transformed as $V_{TS} = R_T \bar{V}_{TS} R_S^\dagger$ and $V_{ST} = R_S \bar{V}_{ST} R_T^\dagger$. With this transformation, the coupling matrices acquire nondiagonal elements in spin space, which means that effectively we have a spin-active interface in which there are spin-flip processes whose probabilities depend on the relative orientation of the impurity spins described by the angle θ.

B. Supercurrent

Our goal is to understand the supercurrent in our two-impurity system. For this purpose, we employ standard nonequilibrium Green's function techniques, see, e.g., Ref. [35], and express the zero-bias current in terms of Keldysh-Green's functions as follows:

$$I_s(\varphi) = \frac{e}{2h} \int_{-\infty}^{\infty} dE \, \mathrm{Tr}[(\sigma_0 \tau_3)(V_{ST} G_{TS}^{+-} - G_{ST}^{+-} V_{TS})], \quad (7)$$

where $\varphi = \phi_T - \phi_S$ is the superconducting phase difference across the junction and $G_{ST/TS}^{+-}$ are Keldysh-Green's functions, which at zero bias can be expressed as $G_{ST/TS}^{+-}(E) = n_F(E)[G_{ST/TS}^a(E) - G_{ST/TS}^r(E)]$. Here, $n_F(E)$ is the Fermi-Dirac distribution at temperature T and for chemical potential set to zero and $G_{ST/TS}^{a/r}(E)$ are advanced/retarded Green's function (GF) that describes the substrate-tip/tip-substrate (ST/TS) hybrid system. These GFs can be obtained via the Dyson equations $G_{ST}^{r/a} = G_{SS}^{r/a} V_{ST} g_{TT}^{r/a}$ and $G_{TS}^{r/a} = g_{TT}^{r/a} V_{TS} G_{SS}^{r/a}$, where the GFs for the tip/substrate (TT/SS) are given by $G_{TT/SS}^{r/a} = [(g_{TT/SS}^{r/a})^{-1} - \Sigma_{S/T}^{r/a}]^{-1}$ with self-energies $\Sigma_S^{r/a} = V_{ST} g_{TT}^{r/a} V_{TS}$ and $\Sigma_T^{r/a} = V_{TS} g_{SS}^{r/a} V_{ST}$. The tip/substrate hybridized GFs can be expressed in terms of the Pauli $\otimes$ Nambu matrices $\sigma_m \tau_n$ as $G_{jj}^{r/a} = \sum_{m,n} G_{jj;mn}^{r/a} \sigma_m \tau_n$,

where $m, n = 0, 1, 2$, and 3. In general, Eq. (7) has to be evaluated numerically. For a small tunneling parameter $t \ll \Gamma_{S/T}$ [35], away from the 0–π transition lines, however, the current-phase relation can be obtained analytically as $I_s \sim \sin\varphi$ (see Appendix A). From a physical point of view, we find that the supercurrent is always carried by four phase-dependent bound states that result from the hybridization of the individual YSR states. Two of these states have negative energies and provide the dominant contribution to the current at low temperatures. The other two states have positive energies and start contributing to the supercurrent flow at higher temperatures.

III. RESULTS AND DISCUSSIONS

In what follows, we illustrate the results for the supercurrent for different ranges of parameters and assume that both superconductors are identical with a gap equal to $\Delta_{S/T}(T) = \Delta_0 \tanh(1.74\sqrt{T_c/T - 1})$ [40]. At $T = 0$ the superconductors (S/T) are characterized by the BCS superconducting gap $\Delta_0 = 1.764 k_B T_c$ with the superconducting critical temperature T_c. For this purpose we define the critical current as $I_c = |I_s(\varphi_{\max})|$, where $|I_s|$ is the maximum at $\varphi = \varphi_{\max}$ such that $0 \leqslant \varphi_{\max} \leqslant \pi$. On the other hand, we characterize the 0 and π phase of supercurrent as $I_s(\varphi_{\max})/I_c > 0$ and $I_s(\varphi_{\max})/I_c < 0$, respectively. Let us start by considering first the limit of low transparency (or weak coupling between the impurities). In Fig. 1(b) we present the results for the zero-temperature critical current as a function of the two exchange fields J_S and J_T for $t = \Delta_0$, $\theta = \pi/2$, $\Gamma_{S/T} = 100\Delta_0$, and $U_{S/T} = 0$ [41]. Notice that there are up to four 0 and π phases separated by boundaries that correspond to the YSR lying at zero energy (for $J_{S/T}/\Gamma_{S/T} = 1$ while $U_{S/T} = 0$). In general, for low transparencies and sufficiently low temperatures, we find that the system exhibits 0 and π phases if $E_{\mathrm{YSR},S\sigma} E_{\mathrm{YSR},T\sigma} > 0$ and $E_{\mathrm{YSR},S\sigma} E_{\mathrm{YSR},T\sigma} < 0$, respectively. In this low transparency regime, the supercurrent is sinusoidal, i.e., $I_s \sim \sin\varphi$, almost for all (J_S, J_T) except near the 0-π transition lines [see Fig. 1(b)], where $I_s(\varphi)$ features higher harmonics, as we shall discuss below. At low temperatures and for low transparencies, the 0-π features of the supercurrent, away from the transition lines, are fairly independent of the value of θ. At low temperatures and for low transparencies, if $U_{S/T} = 0$, the critical current $I_c(J_S, J_T)$ exhibits avoided crossing of the 0-π transition lines at $J_S/\Gamma_S = J_T/\Gamma_T = 1$ for $\theta \neq \pi/2$ or $3\pi/2$, e.g., $\theta = 0$ and π (see Appendix B). The avoided crossings become prominent for finite broadening γ.
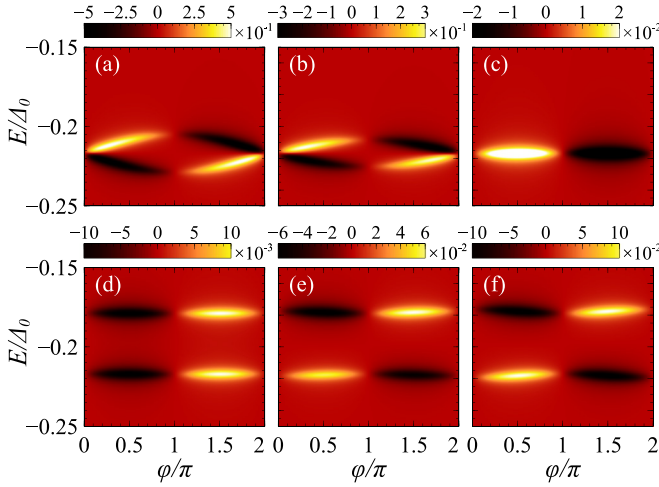
FIG. 2. (a) The spectral current (in color maps), $(\hbar/e)A(E, \varphi)$, for $t = \Delta_0$, $\Gamma_{S/T} = 100\Delta_0$, $U_{S/T} = 0$, and $\gamma = 0.003\Delta_0$ at $T = 0$. Panels (a)–(c) are for $J_S/\Gamma_S = J_T/\Gamma_T = 0.8$ [blue colored diamond shaped point in Fig. 1(b)] and panels (d)–(f) are for $J_S/\Gamma_S = 1.2$ and $J_T/\Gamma_T = 0.8$ [green colored circular shaped point in Fig. 1(b)]. The exchange fields orientation angle θ is set to 0 (a), (d); $\pi/2$ (b), (e); and π (c), (f). Panel (c) exhibits two degenerate bound states due to the symmetry of the two bare systems.

To illustrate the θ and T dependencies of critical current for low transparencies we plot $I_c(\theta, T)$ for $E_{YSR,S\sigma}E_{YSR,T\sigma} > 0$ and $E_{YSR,S\sigma}E_{YSR,T\sigma} < 0$ cases in Figs. 1(c) and 1(d), respectively. We see that I_c increases at low T from $\theta = 0$ to π in Fig. 1(c) and vice versa in Fig. 1(d). Figure 1(c) also illustrates that 0-π transitions (at a fixed θ) can be induced by increasing the temperature for $0 \leqslant \theta < \pi/2$ and $3\pi/2 < \theta \leqslant 2\pi$ if $E_{YSR,S\sigma}E_{YSR,T\sigma} > 0$. On the other hand, a π-0 transition appears in Fig. 1(d) with increasing T for $\pi/2 < \theta < 3\pi/2$ if $E_{YSR,S\sigma}E_{YSR,T\sigma} < 0$. We notice that the critical angle $\theta = \theta_c$, at which a 0-π transition occurs, depends on T. For low transparencies we do not find temperature-induced 0-π transitions for $\theta = \pi/2$ or $3\pi/2$, see Figs. 1(c) and 1(d). Physically, upon increasing the temperature, the positive-energy bound states start to contribute to the supercurrent. It can be shown that the total current carried by the two negative-energy states is in the reverse direction of the total current carried by the two positive-energy states. The 0-π transitions in Figs. 1(c) and 1(d) are due to the enhanced population of the higher energy states with increasing temperature. In Figs. 1(c) and 1(d) we notice that for higher temperatures there are also θ-dependent 0-π transitions.

In what follows, we report spectral current, $A(E, \varphi)$, features at low T and for low transparencies while $J_{S/T} \neq 0$ are away from the transition lines. In general, the supercurrent can be expressed as $I_s(\varphi) = \int dE\, A(E, \varphi)$. At low temperatures, only the two negative-energy bound states of the hybrid system contribute to the supercurrent [see Figs. 2(a)–2(f)]. We find in Fig. 2(a) for $E_{YSR,S\sigma}E_{YSR,T\sigma} > 0$ and $\theta = 0$ that the two negative-energy states carry the current in opposite directions. In this case, it can be shown that they together result in a 0 phase, see, e.g., Fig. 1(c) for $\theta = 0$ at low temperatures. For $E_{YSR,S\sigma}E_{YSR,T\sigma} > 0$ the magnitude of the relative contribution to the supercurrent monotonically increases as θ changes from

0 to π [see Figs. 2(a)–2(c)]. In fact, in this case for $\theta = \pi$ the two negative energy states carry the current in the same direction [see Fig. 2(c)]. Consequently, for $E_{YSR,S\uparrow}E_{YSR,T\uparrow} > 0$ at low T the critical current monotonically increases from $\theta = 0$ to π featuring 0 phases [see Fig. 1(c) at low temperatures]. On the other hand, for $E_{YSR,S\sigma}E_{YSR,T\sigma} < 0$ and $\theta = \pi$ we find in Fig. 2(f) that the two negative energy states carry the current in opposite directions. In this case, it can be shown that they together result in a π-phase, see, e.g., Fig. 1(d) for $\theta = \pi$ at low temperatures. In this case, the magnitude of the relative current increases as θ changes from π to 0 [see Fig. 2(d)–2(f)]. In fact, in this case for $\theta = 0$ the two states carry current in the same direction [see Fig. 2(c)]. Consequently, for $E_{YSR,S\uparrow}E_{YSR,T\uparrow} < 0$ at low T the critical current monotonically increases from $\theta = \pi$ to 0 featuring π phases [see Fig. 1(d) at low temperatures].

Let us remind that usually $I_s \sim \sin\varphi$ for low transparencies, except near the 0-π transition lines in the $I_c(J_S, J_T)$ diagram [see, e.g., Fig. 1(b)]. We now show that at low temperatures higher harmonics in $I_s(\varphi)$ can appear near the 0-π transition lines. Figure 3(a) shows such higher harmonics at the intersection of the transition lines in Fig. 1(b), i.e., for $\theta = \pi/2$ and for $E_{YSR,S\sigma} = E_{YSR,T\sigma} = 0$. The appearance of higher harmonics indicates that there can be supercurrent due to pure (equal spins) triplet pairing. In this case, and despite the fact that $t \ll \Gamma_{S/T}$, we find that the higher powers of tunneling parameters, beyond t^2, significantly contribute to supercurrent. In particular, with the set of parameters in Fig. 3(a), for which $E_{YSR,S\sigma} = E_{YSR,T\sigma} = 0$ and $\theta = \pi/2$, we observe that $I_s(\varphi)$ features a pure second harmonic. At this point, we always find that $I_s(\varphi)$ features a pure second harmonic at low temperatures and for arbitrarily low transparencies. Higher harmonic features for $E_{YSR,S\sigma} = E_{YSR,T\sigma} = 0$ diminish as θ changes from orthogonal to parallel/antiparallel orientations. Figure 3(a) also shows that $I_s(\varphi)$ for $\theta = 0$ and π when $E_{YSR,S\sigma} = E_{YSR,T\sigma} = 0$, which exhibits features of π and 0 phases for $\theta = 0$ and π, respectively. These suggest that for $\theta = 0$ two diagonal π-phase blocks, associated with $E_{YSR,S\sigma}E_{YSR,T\sigma} < 0$, and for $\theta = \pi$ two diagonal 0-phase blocks, associated with $E_{YSR,S\sigma}E_{YSR,T\sigma} > 0$, in $I_c(J_S, J_T)$ diagram would be continuously joined at $J_S/\Gamma_S = J_T/\Gamma_T = 1$ while $U_{S/T} = 0$. Consequently, $I_c(J_S, J_T)$ would exhibit avoided crossing of 0-π transition lines for $\theta = 0$ and π (see Appendix B).

Comparing Figs. 3(b) and 3(d) for $\theta = \pi/2$ and $E_{YSR,S\sigma} = E_{YSR,T\sigma} = 0$, we observe that the bound state crossing in the density of states LDOS $= \text{Im}(\text{Tr}[G_{SS}^a + G_{TT}^a])/16\pi$ is responsible for the onset of pure triplet pairing. The pure triplet pairing amplitude for the substrate in terms of the hybridized GF's components is obtained as $T_{S;\uparrow\uparrow} = |(G_{SS;11}^a - G_{SS;22}^a) - i(G_{SS;12}^a + G_{SS;21}^a)|$. The appearance of pure triplet superconductivity makes $I_s(\varphi)$ nonsinusoidal. Figures 3(b), 3(c), and 3(d) show the LDOS, the substrate's mixed (different spins) triplet pairing amplitude, and the substrate's pure triplet pairing amplitude, respectively, for $\theta = \pi/2$. The substrate's mixed triplet pairing amplitude is obtained in terms of the hybridized GF's components as $T_{S;\uparrow\downarrow} = |(G_{SS;31}^a - iG_{SS;32}^a)|$. In Figs. 3(e)–2(g) we display θ and φ dependencies on zero-energy modes of substrate's singlet pairing, mixed triplet pairing, and pure triplet pairing amplitudes for relatively weak
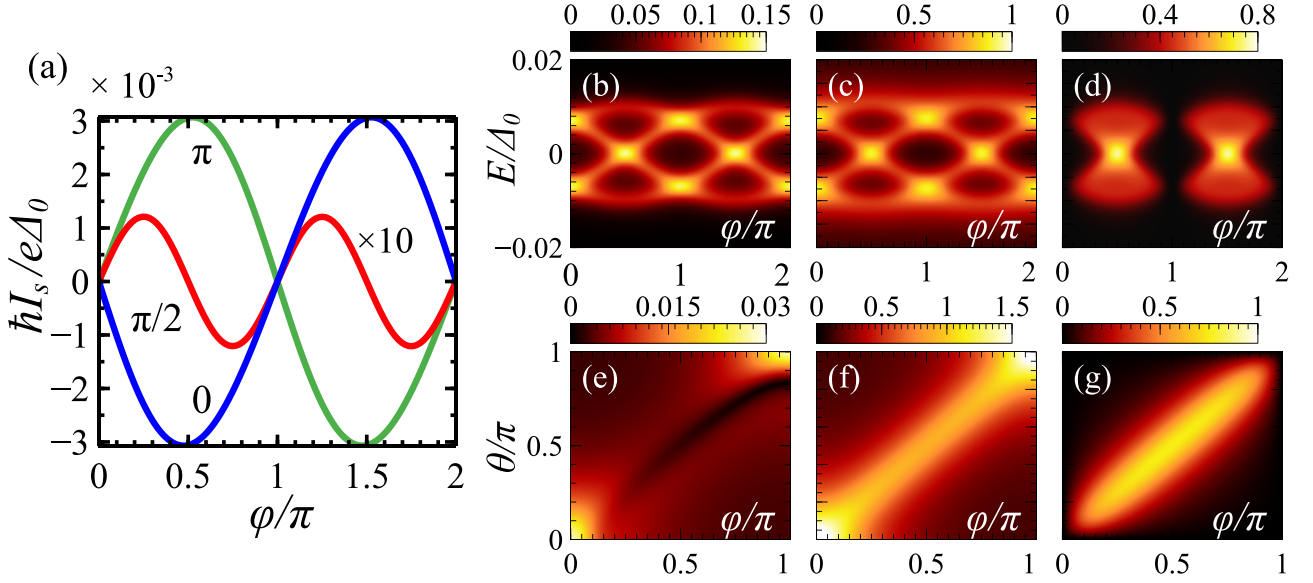
FIG. 3. (a) Current-phase relation $I_s(\varphi)$ for different θ (indicated in the plot), $t = \Delta_0$, $J_S/\Gamma_S = J_T/\Gamma_T = 1$, $\Gamma_{S/T} = 100\Delta_0$, and $U_{S/T} = 0$ at $T = 0$. (b) Local density of states (LDOS), (c) mixed-triplet pairing amplitude, and (d) pure-triplet pairing amplitude for the parameters of the red curve in panel (a). The zero-energy modes of (e) singlet pairing, (f) mixed triplet pairing, and (g) pure triplet pairing amplitudes for $t = \Delta_0$, $J_S/\Gamma_S = J_T/\Gamma_T = 1$, $\Gamma_{S/T} = 100\Delta_0$, and $U_{S/T} = 0$ at $T = 0$. In all panels $\gamma = 0.003\Delta_0$. The quantities with color maps in panels (b)–(g) are expressed in the units of Δ_0^{-1}.

coupling between the impurities, $t = \Delta_0$, setting $J_S/\Gamma_S = J_T/\Gamma_T = 1$, and $U_{S/T} = 0$. The substrate's singlet pairing amplitude in terms of the hybridized GF's components is obtained as $S_{S;\uparrow\downarrow} = |(G^a_{SS;01} - iG^a_{SS;02})|$. We see maximum pure triplet pairing amplitude for $\theta = \pi/2$ and $\varphi = \pi/2$. This features a pure second harmonic in $I_S(\varphi)$ for orthogonal orientation when $E_{\text{YSR},S\sigma} = E_{\text{YSR},T\sigma} = 0$. Higher harmonics and pure triplet features become important for arbitrary $J_{S/T}$ and for all θ when the tunneling parameter t is large.

Finally, we illustrate the contribution of the higher harmonics of $I_s(\varphi)$ in Fig. 4(a) for a higher transparency $t = 70\Delta_0$ and various θ values. The results of Fig. 4(a) were obtained for $J_S/\Gamma_S = J_T/\Gamma_T = 0.8$, which is set away from the 0-π transition lines in $I_c(J_S, J_T)$. We observe that higher harmonics are more prominent for $\theta = \pi/2$. In general, supercurrent

can be expressed in terms of higher harmonics as $I_s(\varphi) = \sum_n I_n \sin(n\varphi)$ with positive integers n. Figure 4(b) shows how the first and second harmonics vary with increasing transparencies t. We clearly see that the second harmonic first enhances with increasing t from low transparencies. For moderate transparencies, the second harmonic plays a significant role in $I_s(\varphi)$. In this case, pure triplet also has a significant contribution to the supercurrent.

IV. CONCLUSIONS

Inspired by recent STM-based experiments, we have presented a theoretical investigation of the DC Josephson effect between two magnetic impurities coupled to superconductors such that they host YSR states. We have shown that the supercurrent in this system exhibits a very rich phenomenology. For instance, for weak coupling between the magnetic impurities, the current-phase relation is sinusoidal, but exhibits various types of 0-π transitions due to changes in the YSR energies, temperature, and orientation of the impurity magnetic moments. Upon increasing the coupling, the current-phase relation becomes nonsinusoidal due to the appearance of (pure) triplet superconductivity. Our results can be tested experimentally in the context of STM and magnetic impurities on superconducting surfaces [34,36].
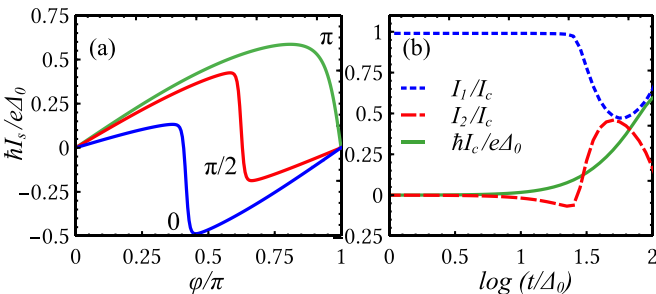

FIG. 4. (a) Zero-temperature current-phase relation for different θ (indicated in the plot), $t = 70\Delta_0$, $\Gamma_{S/T} = 100\Delta_0$, $U_{S/T} = 0$, and $\gamma = 0.003\Delta_0$, and $J_S/\Gamma_S = J_T/\Gamma_T = 0.8$. (b) The first (dotted blue) and second (dashed red) harmonics of the current-phase relation for $\theta = \pi/2$ as a function of the hopping t, as well as the critical current I_c (solid green curve). The rest of the parameters are the same as in panel (a).

APPENDIX A: SUPERCURRENT IN THE TUNNEL REGIME

In the Appendix we elaborate on the analysis of the supercurrent in the tunneling regime and, in particular, we provide some analytical insight into the current-phase relation and the critical current in this regime.

The tip/substrate (TT/SS) bare GFs can be decomposed in the spin $\otimes$ Nambu space as follows:

$$g^a_{jj} = \sum_{l=0,3} \sum_{m=0,3} g^a_{jj;lm} \sigma_l \tau_m + \sum_{l=0,3} \sum_{m=+,-} g^a_{jj;lm} \sigma_l \tau_m, \quad \text{(A1)}$$

with $\tau_\pm = (\tau_1 \pm i\tau_2)/2$ and $g^a_{jj;l\pm} = f^a_{jj;l+} e^{\pm i\phi_j}$. The first and second terms in Eq. (A1) represent the normal and anomalous components of the GF, respectively. In the anomalous part, $f^a_{jj;0+}$ and $f^a_{jj;3+}$ are for the singlet and mixed-triplet contributions, respectively. Using Eq. (7) we can now express the supercurrent for low transparencies as

$$I_s(\varphi) = 8t^2 \frac{e}{h} \sin\varphi \int_{-\infty}^{\infty} dE\, n_F(E) \mathrm{Im}\big[f^a_{SS;0+} f^a_{TT;0+}$$
$$+ f^a_{SS;3+} f^a_{TT;3+} \cos\theta \big]. \quad \text{(A2)}$$

We see that the current-phase relation is sinusoidal $I_s \sim \sin\varphi$ in this limit. Furthermore, we can consider $J_j, \Gamma_j \gg |E_{YSR,j\uparrow}|$ and approximate the denominator of the bare Green's functions as follows

$$D_{j\sigma}(E) \approx -\mathrm{sign}(J_{j\sigma}) \psi_j (E - \mathrm{sign}(J_{j\sigma}) E_{YSR,j\uparrow}), \quad \text{(A3)}$$

where

$$\psi_j = \frac{1}{2\Gamma_j J_j} \big[(J_j^2 - U_j^2 - \Gamma_j^2)^2 + 4\Gamma_j^2 J_j^2 \big]. \quad \text{(A4)}$$

With this approximation, we can obtain the approximate analytical expression of supercurrent for low transparencies as

$$I_s(\varphi) = \left(\frac{8et^2 \Gamma_S \Gamma_T \Delta_S \Delta_T}{h \psi_S \psi_T E^+_{YSR} E^-_{YSR}} \right) [E^+_{YSR} \rho^-_{YSR} \cos^2(\theta/2)$$
$$+ E^-_{YSR}(1 - \rho^+_{YSR}) \sin^2(\theta/2)] \sin\varphi, \quad \text{(A5)}$$

where $E^\pm_{YSR} = E_{YSR,S\uparrow} \pm E_{YSR,T\uparrow}$ and $\rho^\pm_{YSR} = n_F(E_{YSR,S\uparrow}) \pm n_F(E_{YSR,T\uparrow})$. This formula qualitatively captures T and θ dependencies of the supercurrent. At low T, this analytical formula gives a vanishing supercurrent for $\theta = 0$ and $\theta = \pi$ when $E_{YSR,S\uparrow} E_{YSR,T\uparrow} > 0$ and $E_{YSR,S\uparrow} E_{YSR,T\uparrow} < 0$, respectively. This is not correct due to the approximation of $D_{j\sigma}$. The situation is more complicated if $E_{YSR,S\sigma} E_{YSR,T\sigma} = 0$.

In Fig. 5 we present the results for the critical current $I_c = |I_s(\varphi_{\max})|$ computed with Eq. (7) (solid lines) and Eq. (A5) (dashed lines) as a function of the relative orientation θ of the two magnetic impurities at various temperatures. We note
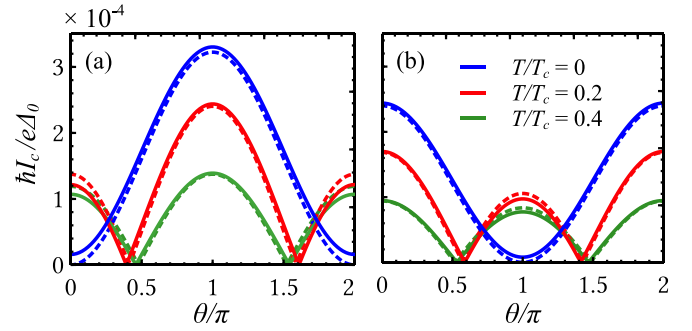

FIG. 5. $I_c(\theta)$ for (a) $J_{S/T}/\Gamma_{S/T} = 0.8$, and (b) $J_S/\Gamma_S = 0.8$ and $J_T/\Gamma_T = 1.2$. For all panels $\Delta_S = \Delta_T$, $\Gamma_{S/T} = 100\Delta_0$, $t = \Delta_0$, $U_{S/T} = 0$, and $\gamma = 0.003\Delta_0$. The solid lines were obtained with Eq. (7) (the exact numerical approach) and the dashed lines correspond to the results obtained with the analytical formula of Eq. (A5).

that $|I_s(\varphi)|$ is maximum at $\varphi = \varphi_{\max}$. For the set of parameters in Fig. 5(a) we find a $0 \to \pi$ phase shift for $0 \leqslant \theta < \pi/2$ and $3\pi/2 < \theta \leqslant 2\pi$ with increasing temperatures for $E_{YSR,S\sigma} E_{YSR,T\sigma} > 0$. For the set of parameters in Fig. 5(b) we find a $\pi \to 0$ phase shift for $\pi/2 < \theta < \pi$ with increasing temperature for $E_{YSR,S\sigma} E_{YSR,T\sigma} > 0$. The analytical formula in Eq. (A5) works well for $J_{S/T}$ values away from the 0-π transition lines in the $I_c(J_S, J_T)$ diagram.

APPENDIX B: CRITICAL CURRENT FOR NONORTHOGONAL ORIENTATIONS

We now consider the behavior of the critical current as a function of the exchange energies $I_c(J_T, J_S)$, for nonorthogonal configurations ($\theta \neq \pi/2$) at zero temperature and for low coupling $t \ll \Gamma_{S/T}$. In Figs. 6(a) and 6(b) we present $I_c(J_S, J_T)$ for $t = \Delta_0$, $\Gamma_{S/T} = 100\Delta_0$, $U_{S/T} = 0$, and for $\theta = 0$ and π, respectively. Usually, for low transparencies and low enough temperatures, we find that the system exhibits 0 and π phases for all θ if $E_{YSR,S\sigma} E_{YSR,T\sigma} > 0$ and $E_{YSR,S\sigma} E_{YSR,T\sigma} < 0$, respectively. However, very close to the 0-π transition lines in $I_c(J_T, J_S)$ the supercurrent features vary with θ [compare Figs. 1(b), 6(a), and 6(b)]. We see that $I_c(J_T, J_S)$ shows dis-
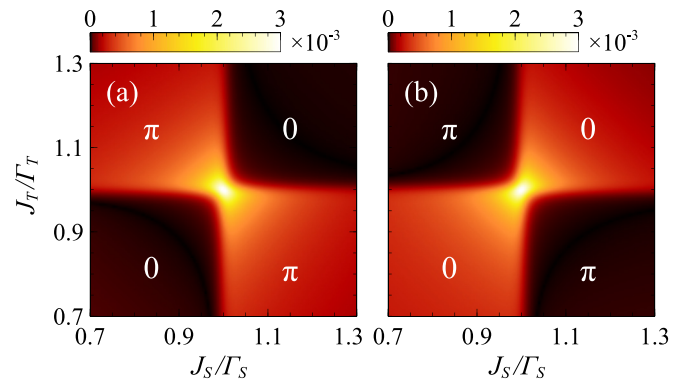

FIG. 6. The zero temperature critical current as a function of J_T and J_S for θ values (a) 0 and (b) π, respectively. For all panels $\Delta_S = \Delta_T$, $\Gamma_{S/T} = 100\Delta_0$, $t = \Delta_0$, $U_{S/T} = 0$, $\gamma = 0.003\Delta_0$, and $T = 0$. The critical currents with color maps in panels (a) and (b) are expressed in the units of $e\Delta_0/\hbar$.

tinct avoided crossing of 0-π transition lines for $\theta = 0$ and π in Figs. 6(a) and 6(b), respectively. This avoided crossing becomes more prominent for finite spectral broadening, γ. In contrast, no avoided crossing happens between the 0-π transition lines for $\theta = \pi/2$ [see Fig. 1(b)]. The magnitude of the current strongly depends on the spin of the hybridized YSR states. For $\theta = 0$ transport through parallel oriented negative energy, YSR states are suppressed due to the spin polarization: Electrons with opposite spins have to virtually

occupy states with very high energy. For $\theta = 0$, the two negative energy YSR states have parallel spins in the 0 phase, where $E_{YSR,S\sigma}E_{YSR,T\sigma} > 0$. In contrast, the two negative energy YSR states have opposite spin in the π phase, where $E_{YSR,S\sigma}E_{YSR,T\sigma} < 0$, which makes the critical current in the π phase larger than in the 0 one, see Fig. 6(a). The situation is reversed for $\theta = \pi$, as illustrated in Fig. 6(a). In the intermediate situation ($\theta = \pi/2$) critical currents for 0 and π phases are identical.

---

[1] B. W. Heinrich, J. I. Pascual, and K. J. Franke, Single magnetic adsorbates on *s*-wave superconductors, Prog. Surf. Sci. **93**, 1 (2018).

[2] D. Choi, N. Lorente, J. Wiebe, K. von Bergmann, A. F. Otte, and A. J. Heinrich, Colloquium: Atomic spin chains on surfaces, Rev. Mod. Phys. **91**, 041001 (2019).

[3] Y. Luh, Bound state in superconductors with paramagnetic impurities, Acta Phys. Sin. **21**, 75 (1965).

[4] H. Shiba, Classical spins in superconductors, Prog. Theor. Phys. **40**, 435 (1968).

[5] A. I. Rusinov, Superconductivity near a paramagnetic impurity, Pis'ma Zh. Eksp. Teor. Fiz. **9**, 146 (1968) [JETP Lett. **9**, 85 (1969)].

[6] A. V. Balatsky, I. Vekhter, and J.-X. Zhu, Impurity-induced states in conventional and unconventional superconductors, Rev. Mod. Phys. **78**, 373 (2006).

[7] K. J. Franke, G. Schulze, and J. I. Pascual, Competition of superconducting phenomena and kondo screening at the nanoscale, Science **332**, 940 (2011).

[8] J. Bauer, J. I. Pascual, and K. J. Franke, Microscopic resolution of the interplay of Kondo screening and superconducting pairing: Mn-phthalocyanine molecules adsorbed on superconducting Pb(111), Phys. Rev. B **87**, 075125 (2013).

[9] L. Malavolti, M. Briganti, M. Hänze, G. Serrano, I. Cimai, G. McMurtrie, E. Otero, P. Ohresser, F. Toi, M. Mannini, R. Sessoli, and S. Loth, Tunable spin-superconductor coupling of spin 1/2 vanadyl phthalocyanine molecules, Nano Lett. **18**, 7955 (2018).

[10] L. Farinacci, G. Ahmadi, G. Reecht, M. Ruby, N. Bogdanoff, O. Peters, B. W. Heinrich, F. von Oppen, and K. J. Franke, Tuning the Coupling of an Individual Magnetic Impurity to a Superconductor: Quantum Phase Transition and Transport, Phys. Rev. Lett. **121**, 196803 (2018).

[11] V. V. Ryazanov, V. A. Oboznov, A. Yu. Rusanov, A. V. Veretennikov, A. A. Golubov, and J. Aarts, Coupling of Two Superconductors through a Ferromagnet: Evidence for a π Junction, Phys. Rev. Lett. **86**, 2427 (2001).

[12] T. Kontos, M. Aprili, J. Lesueur, F. Genêt, B. Stephanidis, and R. Boursier, Josephson Junction through a Thin Ferromagnetic Layer: Negative Coupling, Phys. Rev. Lett. **89**, 137007 (2002).

[13] A. Bauer, J. Bentner, M. Aprili, M. Della Rocca, M. Reinwald, W. Wegscheider, and C. Strunk, Spontaneous Supercurrent Induced by Ferromagnetic π Junctions, Phys. Rev. Lett. **92**, 217001 (2004).

[14] R. Caruso, D. Massarotti, G. Campagnano, A. Pal, H. Ahmad, P. Lucignano, M. Eschrig, M. Blamire, and F. Tafuri, Tuning of Magnetic Activity in Spin-Filter Josephson Junctions Towards Spin-Triplet Transport, Phys. Rev. Lett. **122**, 047002 (2019).

[15] J. W. A. Robinson, S. Piano, G. Burnell, C. Bell, and M. G. Blamire, Critical Current Oscillations in Strong Ferromagnetic π Junctions, Phys. Rev. Lett. **97**, 177003 (2006).

[16] D. Razmadze, R. S. Souto, L. Galletti, A. Maiani, Y. Liu, P. Krogstrup, C. Schrade, A. Gyenis, C. Marcus, and S. Vaitiekenas, Supercurrent reversal in ferromagnetic hybrid nanowire Josephson junctions, Phys. Rev. B **107**, L081301 (2023).

[17] J. A. van Dam, Y. V. Nazarov, E. P. A. M. Bakkers, S. D. Franceschi, and L. P. Kouwenhoven, Supercurrent reversal in quantum dots, Nature (London) **442**, 667 (2006).

[18] S. D. Franceschi, L. Kouwenhoven, C. Schönenberger, and W. Wernsdorfer, Hybrid superconductor-quantum dot devices, Nat. Nanotechnol. **5**, 703 (2010).

[19] A. Martín-Rodero and A. L. Yeyati, Josephson and Andreev transport through quantum dots, Adv. Phys. **60**, 899 (2011).

[20] D. Razmadze, E. O'Farrell, P. Krogstrup, and C. Marcus, Quantum Dot Parity Effects in Trivial and Topological Josephson Junctions, Phys. Rev. Lett. **125**, 116803 (2020).

[21] V. Meden, The Anderson-Josephson quantum dot - a theory perspective, J. Phys.: Condens. Matter **31**, 163001 (2019).

[22] A. Bargerbos, M. Pita-Vidal, R. Žitko, J. vila, L. Splitthoff, L. Grünhaupt, J. Wesdorp, C. Andersen, Y. Liu, L. P. Kouwenhoven, R. Aguado, A. Kou, and B. Heck, Singlet-doublet transitions of a quantum dot josephson junction detected in a transmon circuit, PRX Quantum **3**, 030311 (2022).

[23] K. Grove-Rasmussen, G. Steffensen, A. Jellinggaard, M. H. Madsen, R. Žitko, J. Paaske, and J. Nygård, Yu-Shiba-Rusinov screening of spins in double quantum dots, Nat. Commun. **9**, 2376 (2018).

[24] J. C. Estrada Saldaña, A. Vekris, G. Steffensen, R. Žitko, P. Krogstrup, J. Paaske, K. Grove-Rasmussen, and J. Nygård, Supercurrent in a Double Quantum Dot, Phys. Rev. Lett. **121**, 257701 (2018).

[25] J. C. Estrada Saldaña, A. Vekris, R. Žitko, G. Steffensen, P. Krogstrup, J. Paaske, K. Grove-Rasmussen, and J. Nygård, Two-impurity Yu-Shiba-Rusinov states in coupled quantum dots, Phys. Rev. B **102**, 195143 (2020).

[26] D. Bouman, R. J. J. van, G. Steffensen, D. Pataki, P. Boross, P. Krogstrup, J. Nygård, J. Paaske, A. Pályi, and A. Geresdi, Triplet-blockaded Josephson supercurrent in double quantum dots, Phys. Rev. B **102**, 220505(R) (2020).

[27] A. Vekris, J. C. E. Saldaña, T. Kanne, M. Marnauza, D. Olsteins, F. Fan, X. Li, T. Hvid-Olsen, X. Qiu, H. Xu, J. Nygård, and K. Grove-Rasmussen, Josephson junctions in double nanowires bridged by in-situ deposited superconductors, Phys. Rev. Res. **3**, 033240 (2021).

[28] O. Kürtössy, Z. Scherübl, G. Fülöp, I. Lukács, T. Kanne, J. Nygård, P. Makk, and S. Csonka, Andreev molecule in parallel InAs nanowires, Nano Lett. **21**, 7929 (2021).

[29] G. O. Steffensen, J. C. E. Saldaña, A. Vekris, P. Krogstrup, K. Grove-Rasmussen, J. Nygård, A. L. Yeyati, and J. Paaske, Direct transport between superconducting subgap states in a double quantum dot, Phys. Rev. B **105**, L161302 (2022).

[30] P. Zhang, H. Wu, J. Chen, S. A. Khan, P. Krogstrup, D. Pekker, and S. M. Frolov, Signatures of Andreev Blockade in a Double Quantum Dot Coupled to a Superconductor, Phys. Rev. Lett. **128**, 046801 (2022).

[31] R. Debbarma, M. Aspegren, F. V. Boström, S. Lehmann, K. Dick, and C. Thelander, Josephson current via spin and orbital states of a tunable double quantum dot, Phys. Rev. B **106**, L180507 (2022).

[32] Z. Su, A. B. Tacla, M. Hocevar, D. Car, S. Plissard, E. Bakkers, A. Daley, D. Pekker, and S. M. Frolov, Andreev molecules in semiconductor nanowire double quantum dots, Nat. Commun. **8**, 585 (2017).

[33] S. Karan, H. Huang, C. Padurariu, B. Kubala, G. Morrás, A. Levy Yeyati, J. C. Cuevas, J. Ankerhold, K. Kern, and C. R. Ast, Superconducting quantum interference at the atomic scale, Nat. Phys. **18**, 893 (2022).

[34] H. Huang, C. Padurariu, J. Senkpiel, R. Drost, A. L. Yeyati, J. C. Cuevas, B. Kubala, J. Ankerhold, K. Kern, and C. R. Ast, Tunneling dynamics between superconducting bound states at the atomic limit, Nat. Phys. **16**, 1227 (2020).

[35] A. Villas, R. L. Klees, G. Morrás, H. Huang, C. R. Ast, G. Rastelli, W. Belzig, and J. C. Cuevas, Tunneling processes between Yu-Shiba-Rusinov bound states, Phys. Rev. B **103**, 155407 (2021).

[36] H. Huang, J. Senkpiel, C. Padurariu, R. Drost, A. Villas, R. L. Klees, A. L. Yeyati, J. C. Cuevas, B. Kubala, J. Ankerhold, K. Kern, and C. R. Ast, Spin-dependent tunneling between individual superconducting bound states, Phys. Rev. Res. **3**, L032008 (2021).

[37] D. C. Ohnmacht, W. Belzig, and J. C. Cuevas, Full counting statistics of Yu-Shiba-Rusinov bound states, Phys. Rev. Res. **5**, 033176 (2023).

[38] J. Linder and J. W. A. Robinson, Superconducting spintronics, Nat. Phys. **11**, 307 (2015).

[39] M. Eschrig, Spin-polarized supercurrents for spintronics: A review of current progress, Rep. Prog. Phys. **78**, 104501 (2015).

[40] B. Mühlschlegel, Die thermodynamischen Funktionen des Supraleiters, Z. Phys. **155**, 313 (1959).

[41] As explained in Ref. [36], the analysis of the experimental current-voltage characteristics with the model employed in our work suggests that the impurity spins are freely rotating. That situation can be effectively described for small tunneling parameters t with $\theta = \pi/2$, which gives results that coincide with the current averaged over θ. This is no longer true beyond the tunnel regime, i.e., for larger t values. In this work, we simply treat θ as a model parameter that could be potentially fixed either by magnetic anisotropy in the impurities or by some special kind of magnetic interaction between them.